

# HD 188101: A Spotted B Star with Abundance Anomalies

R. M. Bayazitov<sup>1\*</sup>, L. I. Mashonkina<sup>1,2</sup>, Yu. V. Pakhomov<sup>1</sup>, I. A. Yakunin<sup>3</sup>

<sup>1</sup>*Institute of Astronomy, Russian Academy of Sciences, Moscow, 109017 Russia*

<sup>2</sup>*Institute of Laser Physics, Russian Academy of Sciences, Siberian Branch, Novosibirsk, 630090 Russia*

<sup>3</sup>*Special Astrophysical Observatory, Russian Academy of Sciences, Nizhnii Arkhyz, Karachai-Cherkessian Republic, 369167 Russia*

**Abstract.** Based on spectroscopic and photometric observations, we have determined the fundamental parameters of the poorly studied star HD 188101 with a weak magnetic field. Its effective temperature  $T_{\text{eff}} = 14200 \pm 990$  K and surface gravity  $\log g = 3.70 \pm 0.16$  are typical for main-sequence B9 stars. The He, C, O, Mg, Si, Ti, and Sr abundances have been determined by taking into account the departures from local thermodynamic equilibrium. Overabundances of Si, Ti, and Sr relative to their solar abundances have been revealed. The He abundance is lower than the solar one, but the difference is within the error limits. In addition to the photometric variability known from Kepler data, we have found changes in absorption for He I, Mg II, Si II, Si III, Ti II, and Fe II lines, with different He I and Mg II lines giving different abundances for the same phase of observations. The star HD 188101 is shown to belong to the group of chemically peculiar He-weak SiTiSr stars.

**Keywords:** stars: fundamental parameters, stars: magnetic fields, stars: individual: HD 188101, stars: atmospheres, stars: chemically peculiar

---

\* E-mail: rbayazitov@inasan.ru

## 1. INTRODUCTION

About 10–30% of the main-sequence (MS) B and A stars are chemically peculiar (CP) (I. Romanyuk , 2007; G. Michaud et al., 2015). They show overabundances or underabundances of chemical elements relative to their solar abundances. According to their kinematic characteristics, the CP stars belong to the Galactic thin disk. They rotate around their axis more slowly than do the normal stars. The CP stars with a large-scale magnetic field and periodic variations in brightness with an amplitude of a few hundredths of a magnitude and spectral line profiles belong to the class of Ap–Bp stars.

He-weak (or He-w) stars, in which the He I lines are weaker than those in normal stars of the same spectral type, are distinguished among the CP stars (J. Norris, 1971). About 30 He-weak stars are known (S. Ghazaryan et al., 2019). They are divided into magnetic ones with an overabundance of silicon (Si He-w) and/or titanium and strontium (TiSr Hew) and nonmagnetic ones with an overabundance of phosphorous and gallium (PGa He-w). Weak magnetic fields (E. Borra et al., 1983) and, in some cases, spectroscopic variability were revealed in the SiTiSr subgroup. The subgroup extends the sequence of Ap stars to the range of high temperatures.

The theory of selective diffusion of chemical elements (G. Michaud, 1970) was proposed to explain the observed abundance anomalies. In general, calculations predict the gravitational settling of light elements and the radiative expulsion of heavy elements. The theory contains a large number of parameters and, therefore, requires an observational check.

The star HD 188101 had not aroused any interest of researchers until its light curves with an amplitude of  $0.02^m$  obtained by the Kepler space observatory were published (S. Hümmerich et al., 2018). Such a small amplitude of its brightness variations can be explained by the presence of a spot (or spots) on the surface. The star was included in the program of a search for magnetic fields based on observations with the Main Stellar Spectrograph (MSS) of the Large Azimuthal Telescope (BTA), and a weak magnetic field with a longitudinal component  $B_z$  of less than 1 kG was found in HD 188101 by I. Yakunin et al. (2023). Using the same spectra, I. Yakunin et al. (2023) determined its effective temperature  $T_{\text{eff}} = 14700$  K, surface gravity  $\log g = 3.8$ , and rotational velocity  $V \sin i = 33$  km s<sup>-1</sup> and pointed out that the Si II/Si III ionization balance is upset and it is impossible to describe the He I 4471 Å line profile within the framework of a classical homogeneous model atmosphere under the assumption of local thermodynamic equilibrium (LTE).

Our preliminary analysis of the spectra for HD 188101 showed that the star probably belongs to the small group of He-weak stars that are distinguished by a great variety of abundance anomalies. A detailed abundance analysis, with the abundance determination for a large set of elements from various lines at various ionization stages, is needed to understand the chemical peculiarity mechanisms of He-weak stars. Such information is available in the literature only for very few objects, as can be seen from the catalog data (S. Ghazaryan et al., 2019). Therefore, in this paper we performed a detailed analysis of all the available observational data for a probable new member of the He-weak group, the

star HD 188101, to refine its atmospheric parameters, to determine the abundances for the maximum possible number of chemical elements, including, given the departures from LTE, those for He, C, O, Mg, Si, Ti, and Sr, to investigate the variability in lines and continuum, and to establish the type of chemical peculiarity.

In Section 2 we present the sources of observational data, the variability of the equivalent widths of spectral lines, and the analysis of longitudinal magnetic field measurements. The spectrum modeling methods, including the construction of a model He I atom, are described in Section 3. The atmospheric parameters and chemical composition are determined in Sections 4 and 5. Our results are discussed in Section 6.

## 2. OBSERVATIONAL DATA

### *2.1. Distance, Photometry, and Spectra*

The latest Gaia data release (Gaia DR3, Gaia Collaboration, 2021) gives a parallax  $\pi = 2.34 \pm 0.93$  (RUWE = 2.77) for HD 188101. RUWE (renormalized unit weight error) is the factor that characterizes the reliability of the Gaia parallax. For reliable values RUWE should be less than 1.4. Despite the high value of RUWE, we used the Gaia DR3 parallax. Note that the parallaxes in the first Hipparcos catalogue ( $\pi = 2.31 \pm 0.77$ , The HIPPARCOS and TYCHO catalogues, 1997) and Gaia DR3 coincide within the error limits.

We used the photometric data<sup>1 2</sup> in the range from 1000 Å to 20 μm obtained with various instruments<sup>3</sup> (Table 1). To investigate the variability, we extracted the Kepler photometric data from the archive and processed them following the instructions<sup>4</sup>.

We used the MSS spectra with a resolution  $R = \lambda/\Delta\lambda = 15000$  and a signal-to-noise ratio  $S/N = 150\text{--}200$  in the spectral ranges 4420–4990 Å or 4490–5055 Å. We also used the spectrum taken with the echelle spectrograph at the Nasmyth focus of BTA (NES) with  $R = 40000$  and  $S/N = 50$  in the range 3950–6880 Å. Table 2 gives a log of spectroscopic observations. Here and below, the phases were obtained using the ephemeris  $JD = 2455681.4953 + 3.98726E$  from I. Yakunin et al. (2023).

### *2.2. Line Intensity Variability*

In this section we investigate the variability of the longitudinal magnetic field  $B_z$  measured by I. Yakunin et al. (2023) from the MSS spectra and the equivalent widths of spectral lines.

---

<sup>1</sup><https://vizier.cds.unistra.fr/viz-bin/VizieR>

<sup>2</sup><https://astroquery.readthedocs.io/en/latest/>

<sup>3</sup><https://vizier.cds.unistra.fr/vizier/welcome/vizierbrowse.gml?bigcat>

<sup>4</sup><https://lightkurve.github.io/lightkurve/tutorials/1-getting-started/using-light-curve-file-products.html?highlight=tesslightcurve>

Table 1: The filters with their effective wavelengths and references to the catalogs

$\lambda_{\text{eff}}$ (Å)	Filter	Catalog	Reference
1565.54	TD1/WIDE.1565	II/59B/catalog	G. Thompson et al. (1978)
1959.68	TD1/WIDE.1965		
2358.45	TD1/WIDE.2365		
2737.17	TD1/WIDE.2740		
4901.70	Hipparcos.Hp	I/311/hip2	The HIPPARCOS and TYCHO catalogues (1997)
5035.75	GAIA3.Gbp	I/355/gaiadr3	Gaia Collaboration (2022)
5822.39	GAIA3.G		
7619.96	GAIA3.Grp		
4810.16	PAN-STARRS/PS1.g	II/349/ps1	K. Chambers et al. (2016)
6155.47	PAN-STARRS/PS1.r		
7503.03	PAN-STARRS/PS1.i		
8668.36	PAN-STARRS/PS1.z		
9613.60	PAN-STARRS/PS1.y		
12350.00	2MASS.J	II/246/out	R. Cutri et al. (2003)
16620.00	2MASS.H		
21590.00	2MASS.Ks		
33526.00	WISE.W1	II/311/wise	R. Cutri et al. (2012)
46028.00	WISE.W2		
115608.00	WISE.W3		
220883.00	WISE.W4		

To analyze the change in the longitudinal magnetic field  $B_z$  measured by I. Yakunin et al. (2023), we used the model of a central magnetic dipole. It is characterized by the magnetic field at the pole of the dipole  $B_p$  and the inclination of the dipole axis to the stellar rotation axis  $\beta$  (it changes from  $0^\circ$  to  $180^\circ$ ). The inclination of the rotation axis to the line of sight  $i = 42^\circ$  was calculated using the period of the photometric variability  $P = 3.98726$  days and  $V \sin i$  from I. Yakunin et al. (2023). Positive values of  $B_z$  are observed over the entire rotation period and, therefore, the magnetic pole cannot disappear from the visible stellar disk. Taking  $\beta = 30^\circ$ , we obtained an upper limit,  $B_p = 3$  kG, allowing the atmosphere to be modeled without taking into account the magnetic field (such magnetic fields change the temperature in the atmosphere by less than 100 K; (O. Kochukhov et al., 2005)). Note that the observations are not described by the magnetic dipole model; we estimate only the upper limit for  $B_p$ .

Consider the variability in spectral lines. When the MSS spectra are analyzed, the equivalent widths presented in Figs. 1 and 2 give reliable information about the variability. The strongest, unblended Mg II, He I, Si III, Ti II, and Fe II lines are shown. The remaining lines of these species exhibit a similar behavior. The minima and maxima are seen to occur at phases 0.4 and 0.9. The changes in the Si II, Si III, Ti II, and Fe II lines are out of phase with those in the He I 4713 Å and Mg II 4481 Å, lines, but are in phase with the light curve. We know peculiar stars in which an anticorrelation of the absorptions in He I and Si II lines (A. Deutsch, 1952) and a correlation of the Mg and He abundances

Table 2: Log of spectroscopic observations of HD 188101 with MSS and NES

Date	JD 245...	Rotation phase	Range, Å
MSS			
03.04.19	8577.5409	0.325	4436-4993
26.04.19	8600.5416	0.093	4494-5050
16.05.19	8620.3812	0.069	4498-5054
17.05.19	8621.4375	0.334	4498-5054
20.05.19	8624.4812	0.097	4498-5054
20.10.19	8777.3298	0.432	4425-4982
21.10.19	8778.3361	0.684	4425-4982
11.11.19	8799.2812	0.937	4425-4982
14.11.19	8802.2541	0.683	4425-4982
17.11.19	8805.1486	0.408	4425-4982
05.06.20	9006.4236	0.888	4425-4982
29.07.20	9060.3083	0.402	4425-4982
30.07.20			
04.09.20			
NES			
12.10.19	8769.2721	0.411	3948-6981

(G. Topil’skaya, 1993). are observed. The photometric variability and the change in line absorption with stellar rotation phase point to abundance inhomogeneities in the surface layers.

Note that we analyze the object as a single one. First, within the limits of errors  $\simeq 8$  km s<sup>-1</sup>, we found no changes in the radial velocity. Second, the period of the photometric variability, 4 days, is too short for the star to be a binary.

### 3. SPECTRUM MODELING METHODS

#### 3.1. Codes and Methods of Calculations

The statistical equilibrium and radiative transfer equations are solved using the DETAIL code (J. Giddings, 1981; K. Butler, 1984; N. Przybilla et al., 2011). The model atom and the model atmosphere serve as the input parameters; the level populations relative to the LTE values serve as the output ones. Plane-parallel, homogeneous model atmospheres were computed by the LLmodels code (line-by-line, D. Shulyak et al., 2004) with a detailed allowance for the absorption in lines at a specified individual chemical composition of the star. Table 3 lists the species whose lines we analyze when abandoning LTE.

We determined the abundances of chemical elements by the synthetic spectrum method, i.e., by fitting the observed lines by theoretical profiles. The synthetic spectrum was computed using the SynthVb code (V. Tsymbal et al., 2019). For the lines of

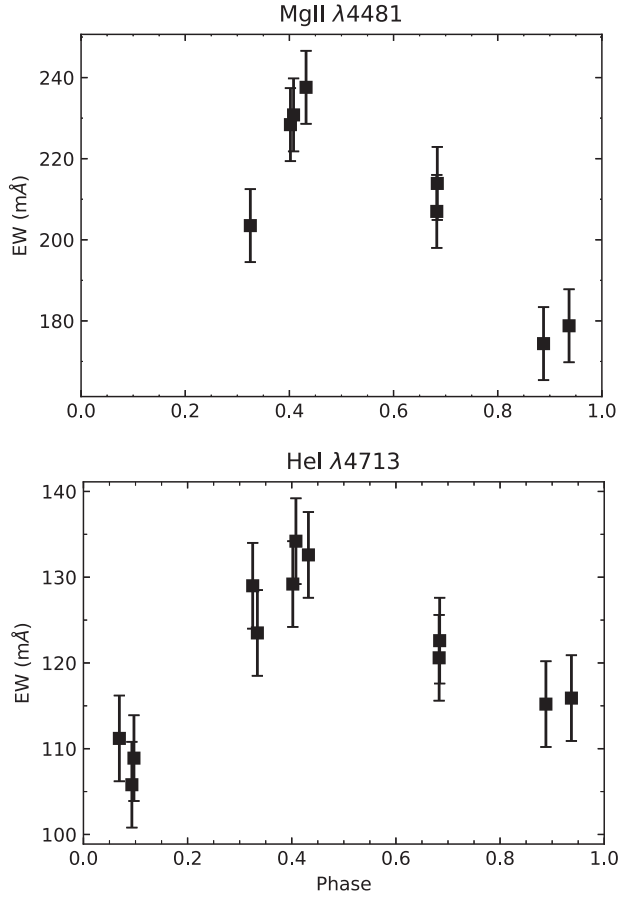


Figure 1: Changes in the equivalent widths of the Mg II and He I lines in HD 188101 with rotation phase.

the atom under study SynthVb uses the  $b$ -factors computed by DETAIL; for the remaining lines we assume LTE. For a specific level  $b_i = n_i^{\text{NLTE}}/n_i^{\text{LTE}}$  characterizes the deviation of the population from the equilibrium one. Here,  $n_i^{\text{NLTE}}$  and  $n_i^{\text{LTE}}$  are the level populations obtained when solving the statistical equilibrium equations and from the Saha-Boltzmann formulas, respectively. The atomic data needed to compute the synthetic spectrum were taken from the Vienna Atomic Line Database<sup>5</sup> (VALD, T. Ryabchikova et al. , 2015). The BinMag6 code (O. Kochukhov, 2018) is used for the comparison with observations.

### 3.2. Model He I atom

B-type stars are young objects, and the He abundance in them should coincide with the cosmic one. The protosolar value,  $\log \varepsilon_{\text{He}} = 10.994 \pm 0.02$  (K. Lodders, 2021), and the mean abundance for a sample of B stars,  $\log \varepsilon_{\text{He}} = 10.99 \pm 0.01$  (M.-F. Nieva, N. Przybilla, 2012), may be considered as a standard cosmic He abundance. Here, we use the scale  $\log \varepsilon_{\text{el}} = \lg N_{\text{el}}/N_{\text{H}} + 12$ , where  $N_{\text{el}}$  and  $N_{\text{H}}$  are the number densities of the atoms under study and hydrogen, respectively. The deviation of the He abundance in a star from the

<sup>5</sup><https://vald.inasan.ru/vald3/php/vald.php>

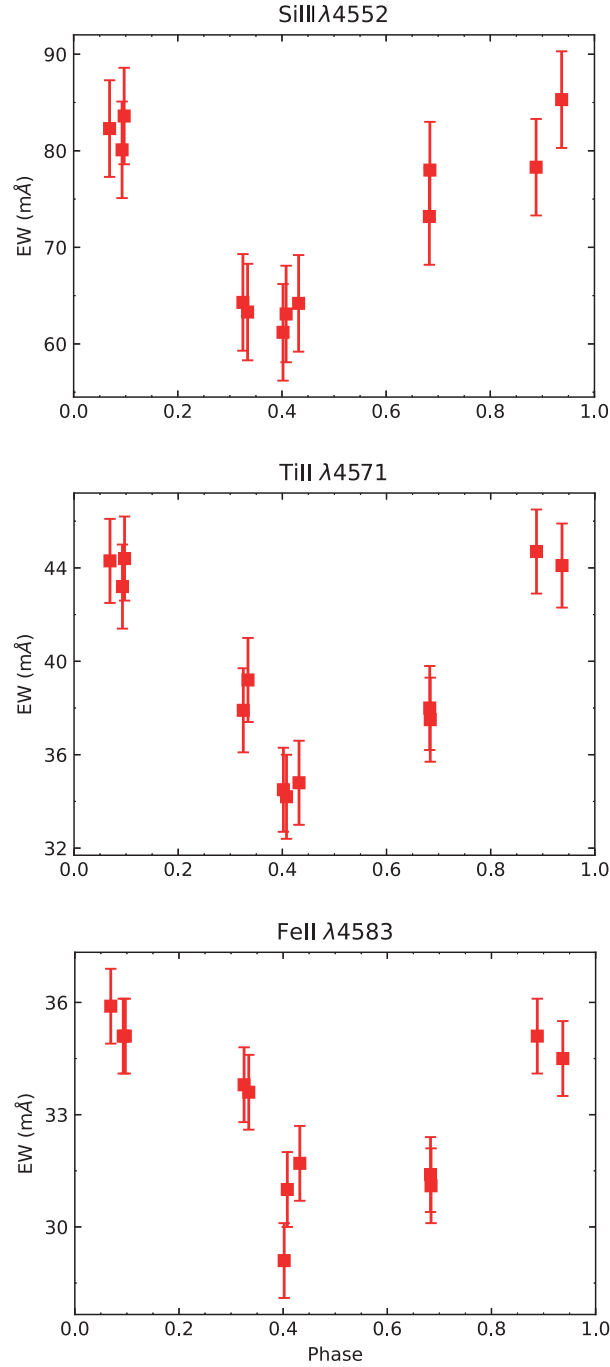


Figure 2: Changes in the equivalent widths of the Si III, Ti II, and Fe II lines in HD 188101 with rotation phase.

cosmic one is an indicator of the action of chemical separation mechanisms in the surface layers. To increase the accuracy of the He abundance in the atmosphere of HD 188101, we used an approach based on the abandonment of the assumption of LTE (a non-LTE approach). For this purpose, we constructed a model He I atom.

*Energy levels.* The model atom was constructed using the singlet and triplet levels of the He I  $1snl$  electronic configurations with  $n \leq 7$  and  $l \leq 6$  from the NIST experimental

Table 3: Model atoms

Atom	Reference
He I	This paper
C I-II	S. Alexeeva et al. (2016)
O I	T. Sitnova et al. (2013)
Mg I-II	S. Alexeeva et al. (2018)
Si I-III	L. Mashonkina (2020)
Ti I-II	T. Sitnova et al. (2020)
Sr II	L. Mashonkina et al. (2020)

database NIST<sup>6</sup> (A. Kramida et al., 2022). The system of He I levels was supplemented by the ground He II state. The fine splitting of the triplet states is ignored due to the small energy separation, less than  $10^{-4}$  eV. The uppermost He I levels are separated from the continuum by 0.28 eV, which is less than the mean thermal energy of electrons in the atmospheres of B stars, and the electron-impact ionization and recombination processes provide a close relationship between the two helium ionization stages. The levels of the model atom are shown in Fig. 3.

*Radiative transitions.* For the levels with an orbital angular momentum  $L = S, P$  and  $D$  the photoionization cross sections  $\sigma_{ph}(\text{OP})$  calculated within the Opacity Project were taken from TOPbase<sup>7</sup> (W. Cunto et al., 1993). The  $np^3P^\circ$  levels with  $n = 4, 5, 6$  and  $7$ , for which there are no data in TOPbase, are exceptions. For the remaining levels we used the hydrogen-like photoionization cross sections. For the levels with  $\sigma_{ph}(\text{OP})$  our comparisons showed that the hydrogen-like cross sections could be close to  $\sigma_{ph}(\text{OP})$ , for example, for the  $2p^3P^\circ$  level, be larger than  $\sigma_{ph}(\text{OP})$ , for the  $2p^1P^\circ$  level, and be considerably smaller than  $\sigma_{ph}(\text{OP})$ , for the  $2s^3S$  level.

The photoionization cross sections for the He I levels, including the  $np$  and  $nf$  levels absent in TOPbase, were calculated by S. N. Nahar (2010) using the same method as that in the Opacity Project, and the data are presented in NORAD<sup>8</sup>. Our comparisons showed that the TOPbase and NORAD data agree for the common levels. However, since  $\sigma_{ph}(\text{NORAD})$  are available for a larger set of levels, below we carried out test calculations to estimate the influence of the substitution of  $\sigma_{ph}(\text{NORAD})$  for the hydrogen-like cross sections on the non-LTE results.

The model He I atom includes 183 allowed transitions. The oscillator strengths  $f_{ij}$  were taken from NIST and the atomic structure calculations by R. Kurucz<sup>9</sup>. For 14 transitions the radiative rates are calculated with the Stark absorption profile from (A. J. Barnard et al., 1974, He I 4471 Å) and (H. R. Griem, 1974, the remaining 13 transitions). We use the Voigt absorption profile for the transitions with  $f_{ij} > 0.01$  in the range 900–6000 Å and the Doppler one for the remaining transitions.

<sup>6</sup><https://www.nist.gov/pml/atomic-spectra-database>

<sup>7</sup><https://cds.unistra.fr/topbase/topbase.html>

<sup>8</sup><https://norad.astronomy.osu.edu/>

<sup>9</sup><http://kurucz.harvard.edu/>

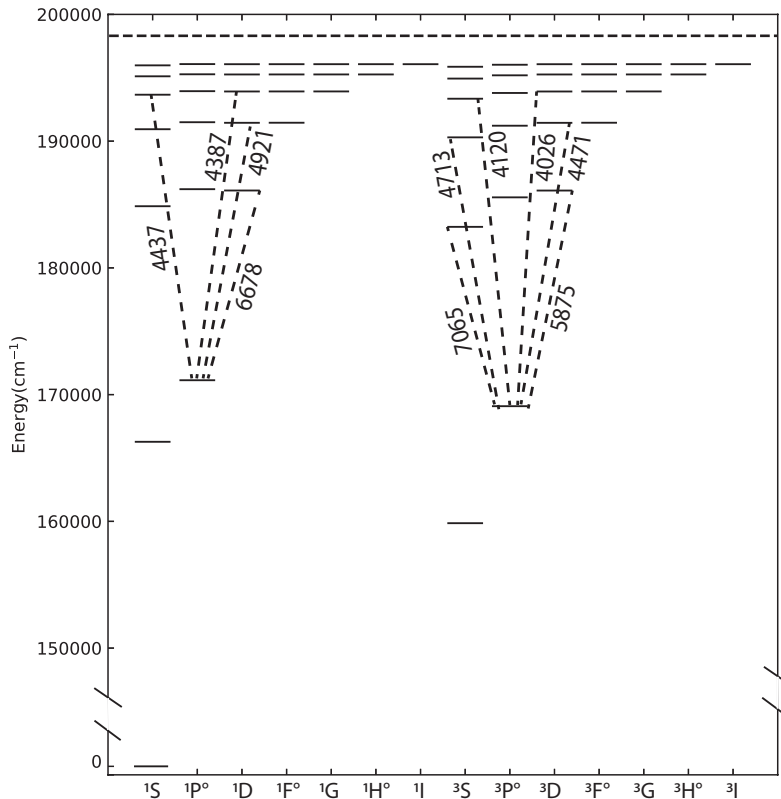


Figure 3: Energy levels in the model He I atom. The dashes indicate the transitions in which the lines involved in determining the He abundance are formed (the wavelengths are in Å).

*Transitions under the action of collisions with electrons.* For 196 bound-bound (b-b) transitions between levels with  $n \leq 5$  we use the effective collision strengths  $\Upsilon$  calculated by I. Bray et al. (2000) and P. Sawey, K. Berrington (1993). For the remaining transitions we use the semiempirical formula from H. van Regemorter (1962) if the transition is allowed and take  $\Upsilon = 1$  if the transition is forbidden.

The electron-impact ionization cross sections are calculated using the formula from M. J. Seaton (1962).

### 3.3. Non-LTE Effects for He I and Testing the Model Atom

Before using the constructed model atom to analyze the He I lines in HD 188101, we tested it by determining the He abundance in chemically normal stars for which non-LTE calculations were carried out. We chose two stars with the solar chemical composition from our previous papers: 21 Peg with  $T_{\text{eff}} = 10400$  K,  $\log g = 3.5$  (10400/3.5), and a microturbulent velocity  $v_{\text{mic}} = 0.5$  km s $^{-1}$  and  $\iota$  Her with 17500/3.8 and  $v_{\text{mic}} = 1.05$  km s $^{-1}$ .

The details of determining the atmospheric parameters and the ESPaDOnS spectra<sup>10</sup> being used can be found, for example, in (L. Mashonkina et al., 2020).

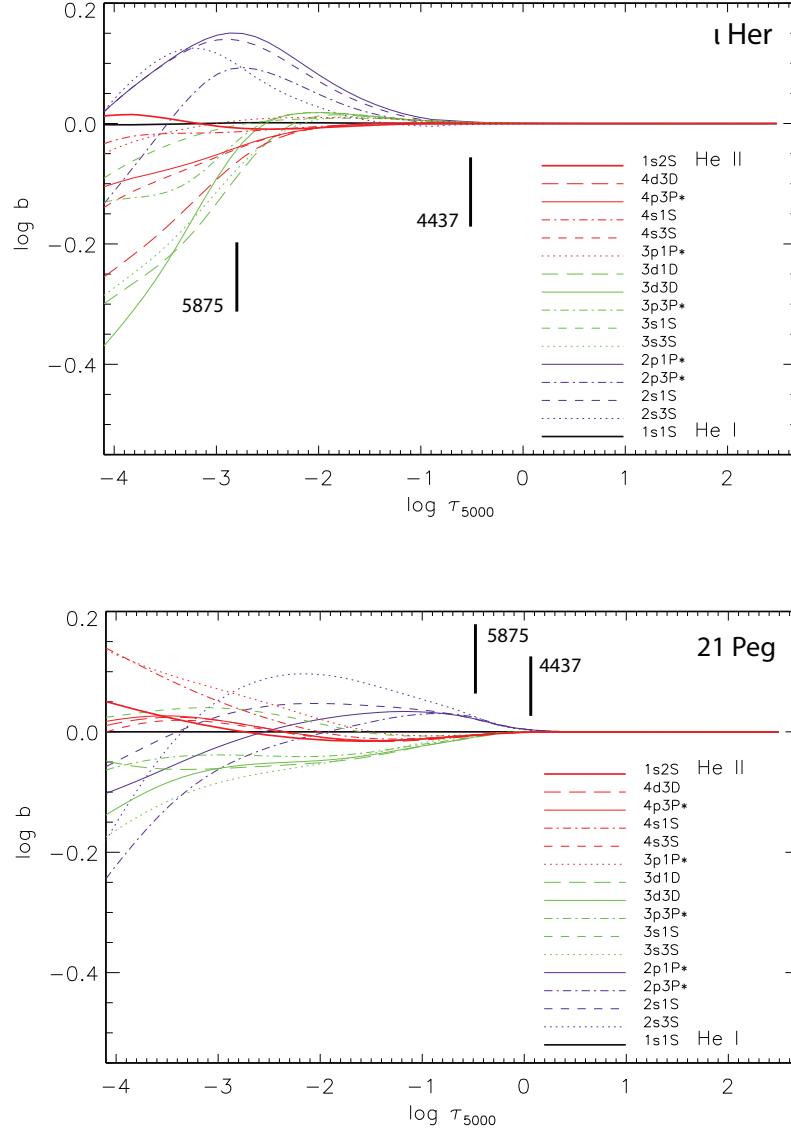


Figure 4: The  $b$ -factors of He I and He II levels as a function of the depth in the 17 500/3.8 ( $\iota$  Her, the upper panel) and 10 400/3.5 (21 Peg, the lower panel) model atmospheres. The formation depths of the He I 4437 and 5875 Å line cores are indicated.

Figure 4 shows the  $b$ -factors of He I levels calculated for the model atmospheres of 21 Peg and  $\iota$  Her. In both models the neutral helium atoms dominate in the total helium number density and, therefore, for the ground He I state there are no departures from LTE ( $b = 1$ ) at all depths. The lower levels of those transitions in which the observed lines are formed (Table 4), namely  $2s\ ^1S$ ,  $2p\ ^1P^\circ$  and  $2p\ ^3P^\circ$ , are overpopulated ( $b_{low} > 1$ ) relative to the equilibrium populations in the line formation region, while the upper levels are overpopulated, but to a lesser degree than the lower ones ( $b_{up} > 1$ ,  $b_{up} < b_{low}$ ) for  $\iota$  Her and underpopulated ( $b_{up} < 1$ ) for 21 Peg. The slight excess of the photoionization

<sup>10</sup><https://www.cadc-ccda.hia-ihh.nrc-cnrc.gc.ca/en/search/>

rate compared to the photorecombination rate for the ground state, the strong coupling of highly excited states with the continuum, and the spontaneous transitions to lower-lying levels are responsible for this He I level population picture.

In the line formation region  $b_{low} > 1$  and  $b_{up}/b_{low} < 1$  for all of the transitions in Table 4. The lines strengthen compared to LTE, and a lower abundance is required to describe the observations. Thus, the non-LTE abundance corrections  $\Delta_{NLTE} = \log \varepsilon_{NLTE} - \log \varepsilon_{LTE}$  are negative.

The abundances derived from individual lines in 21 Peg and  $\iota$  Her are given in Table 4 for various line formation scenarios – LTE and non-LTE using the Voigt (NLTE Voigt) and Stark (NLTE Stark) profiles in our calculations of the radiative rates. We also carried out non-LTE calculations using  $\sigma_{ph}$ (NORAD). The abundance difference between the cases of  $\sigma_{ph}$ (OP) and  $\sigma_{ph}$ (NORAD) did not exceed 0.01 dex for any of the lines. This is because the photoionization and photorecombination processes associated with the He I  $4p^3P^o$  level and higher levels play a minor role in the mechanism of departures from LTE. It turned out that the He I 4921, 5015, 5875, 6678, 7065 and 7282 Å line profiles for  $\iota$  Her could not be reproduced in the LTE calculations. NLTE Voigt and NLTE Stark yield very close results with a maximum abundance difference of 0.01 dex for 21 Peg and 0.02 dex for  $\iota$  Her. The non-LTE corrections (NLTE Stark – LTE) for individual lines lie within the ranges from  $-0.01$  to  $-0.13$  dex for 21 Peg and from 0 to  $-0.08$  dex for  $\iota$  Her. For 21 Peg, for which the LTE and non-LTE abundances were determined for each of the lines, using the non-LTE approach allows one to reduce the abundance error  $\sigma = \sqrt{\sum(x - \bar{x})^2 / (N_l - 1)}$  by a factor of 1.5. Here,  $N_l$  is the number of lines.

In the universally accepted scale we obtained the non-LTE abundance  $\log \varepsilon_{He} = 10.94 \pm 0.04$  for 21 Peg and  $\log \varepsilon_{He} = 10.95 \pm 0.03$  for  $\iota$  Her. These values agree, within the error limits, with the standard cosmic abundance  $\log \varepsilon_{He} = 10.99 \pm 0.02$  (K. Lodders, 2021).

*Comparison with other authors.* The departures from LTE in He I lines were investigated in many papers (see, e.g., L. Auer and D. Mihalas, 1973; P. Dufton, C. McKeith, 1980; D. Husfeld et al., 1989; N. Sakhibullin and W. Schabert, 1990; Y. Takeda, 1994; F. Leone et al., 1995; N. Przybilla, 2005; S. Korotin and T. Ryabchikova, 2018). A direct comparison with the results of S. Korotin and T. Ryabchikova (2018), who performed their calculations for 21 Peg and  $\iota$  Her using the same atmospheric parameters as those in our paper, can be made. For 21 Peg and the He I 5875 and 6678 Å lines with maximum departures from LTE S. Korotin and T. Ryabchikova (2018) obtained amore negative non-LTE correction,  $\Delta_{NLTE} = -0.17$  dex compared to our  $\Delta_{NLTE} = -0.13$  and  $-0.12$  dex. As a consequence, for both stars S. Korotin and T. Ryabchikova (2018) obtained a lower mean He abundance, by 0.04 dex.

#### 4. DETERMINATION OF $T_{eff}$ AND $\log g$

We determined  $T_{eff}$  from photometry and  $\log g$  from Balmer hydrogen lines and evolutionary tracks. The interstellar extinction data were extracted from various maps

Table 4: LTE and non-LTE helium abundances  $\lg N_{\text{He}}/N_{\text{tot}}$  in the atmospheres of the standard stars 21 Peg and  $\iota$  Her.

$\lambda(\text{\AA})$	$\lg gf$	Transition	21 Peg			$\iota$ Her		
			LTE	NLTE Voigt	NLTE Stark	LTE	NLTE Voigt	NLTE Stark
4026	-0.37	$2p^3P^\circ - 5d^3D$	-1.08	-1.10	-1.10	-1.10	-1.10	-1.10
4120	-1.47	$2p^3P^\circ - 5s^3S$	-1.06	-1.08	-1.08	-1.05	-1.08	-1.09
4387	-0.89	$2p^1P^\circ - 5d^1D$	-1.11	-1.12	-1.12	-0.99	-1.05	-1.05
4437	-2.02	$2p^1P^\circ - 5s^1S$	-1.06	-1.07	-1.07	-1.04	-1.07	-1.08
4471	0.44	$2p^3P^\circ - 4d^3D$	-1.09	-1.14	-1.14	-1.03	-1.09	-1.11
4713	-1.02	$2p^3P^\circ - 4s^3S$	-1.13	-1.15	-1.16	-1.07	-1.14	-1.15
4921	-0.44	$2p^1P^\circ - 4d^1D$	-1.04	-1.07	-1.07	:: <sup>1</sup>	-1.02	-1.03
5015	-0.82	$2s^1S - 3p^1P^\circ$				::	-1.07	-1.09
5875	0.74	$2p^3P^\circ - 3d^3D$	-0.96	-1.09	-1.09	::	-1.07	-1.09
6678	0.33	$2p^1P^\circ - 3d^1D$	-0.99	-1.11	-1.11	::	-1.11	-1.12
7065	-0.20	$2p^3P^\circ - 3s^3S$	-0.93	-1.03	-1.03	::	-1.10	-1.12
7281	-0.84	$2p^1P^\circ - 3s^1S$				::	-1.06	-1.08
		Mean	-1.05	-1.10	-1.10	-1.05	-1.08	-1.09
		$\sigma(\text{dex})$	0.06	0.03	0.04	0.03	0.03	0.03

<sup>1</sup> It is impossible to reproduce the observed profile.

(F. Arenou et al. , 1992; G. Green et al., 2019; G. Gontcharov, 2017; R. Lallement et al., 2022, – Arenou+1992, Green+2019, Gontcharov 2017, Lallement+2022, respectively). From the Green+2019 maps<sup>11</sup> we determined the color excess  $E(g-r) = 0.050^{+0.054}_{-0.050}$ , using the Bayestar2019 version. For the conversion to the color excess in the Johnson system we took the coefficients suitable for the object under study from M. Fukugita et al. (1996),  $E(B-V) = E(g-r)/1.05$ . The Lallement+2022 maps<sup>12</sup> give  $A_V = 0.067^{+0.032}_{-0.019}$ . Using the interstellar extinction law  $R_V \times A_\lambda/A_V$  with  $R_V = 3.1$  from J. Mathis (1990), we found the color excess  $E(B-V)$ . It can be seen from Table 5 that different maps give color excesses from 0.02 to 0.08. To calculate the uncertainty in the color excess, we took into account the error in  $E(B-V)$  given by the maps and the uncertainty in the distance to the star (see Table 7).

Table 5: The color excesses  $E(B-V)$  determined from four interstellar extinction maps

Arenou+1992	Green+2019	Goncharov 2017	Lallement+2022
$0.051^{+0.065}_{-0.049}$	$0.048^{+0.051}_{-0.048}$	$0.081^{+0.041}_{-0.016}$	$0.022^{+0.010}_{-0.006}$

$T_{\text{eff}}$  and the angular diameter  $\theta$  were determined by minimizing the deviations of the theoretical fluxes  $F_\lambda$  convolved with the filter transmission curves<sup>13</sup>, from the extinction-corrected observed fluxes. The fluxes  $F_\lambda$  were computed by the LLmodels code for a set of

<sup>11</sup><http://argonaut.skymaps.info/>

<sup>12</sup><https://explore-platform.eu>

<sup>13</sup><https://svo2.cab.inta-csic.es/theory/fps3/index.php?mode=voservice>

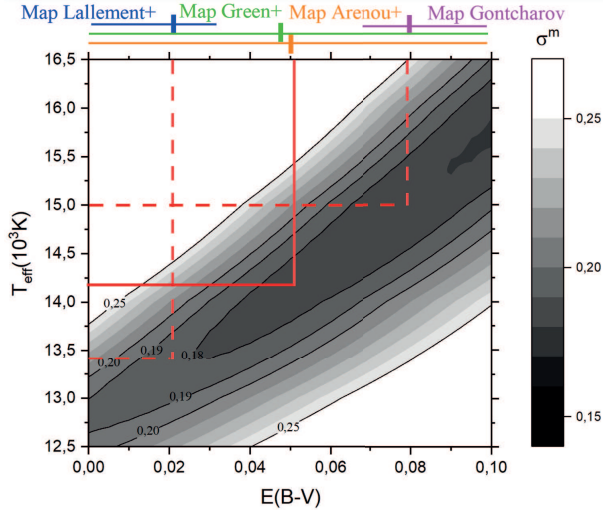


Figure 5: The deviations of the theoretical fluxes from the observed ones (in magnitudes) for different  $T_{\text{eff}}$  and  $E(B-V)$  are indicated by the shading with different intensities. The solid and dashed red straight lines mark the derived  $E(B-V)$  and  $T_{\text{eff}}$  with their errors.

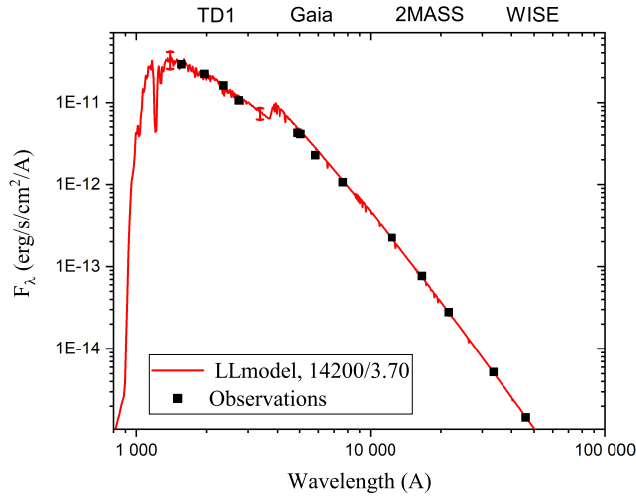


Figure 6: The observed fluxes corrected for interstellar extinction (squares) and the theoretical fluxes smoothed by a Gaussian with a FWHM of  $10 \text{ \AA}$  (curve) for the model with the ultimately adopted atmospheric parameters. The bar of the theoretical flux indicates the error due to the uncertainty in the effective temperature  $\sigma_O$ .

$T_{\text{eff}}$  at fixed  $\log g = 4.0$  and solar chemical composition. Figure 5 shows the deviations from the observations in magnitudes,  $\sigma^m = \sqrt{\sum_{i=1}^{N_{\text{obs}}} (m_i^{\text{syn}} - m_i^{\text{obs}})^2 / N_{\text{obs}}}$  for a set of  $E(B-V)$  and  $T_{\text{eff}}$ , and the color excesses with their errors corresponding to HD 188101 on different maps are marked. The minimum deviation  $\sigma^m = 0.17$  was found in the ranges of  $E(B-V)$  from 0.09 to 0.16 and  $T_{\text{eff}}$  from 15500 to 18000 K. However, in view of the degeneracy in  $E(B-V)$  and  $T_{\text{eff}}$  we fixed  $E(B-V) = 0.05 \pm 0.03$  based on the interstellar extinction maps. We determined  $T_{\text{eff}}$ ,  $\theta$  and the errors related to the uncertainties in the color excess  $\sigma_E$  and surface gravity  $\sigma_g$ . The errors attributable to the observations  $\sigma_O$  were estimated by the Monte Carlo method for  $T_{\text{eff}}$  and by calculating the standard deviation from the

observations for the angular diameter. The total error is calculated as  $\sigma_{atm}^2 = \sigma_E^2 + \sigma_g^2 + \sigma_O^2$ . In addition, we estimated the influence of the overabundances of some chemical elements ( $[\text{Si}/\text{H}] \simeq 1.0$ ,  $[\text{Ti}/\text{H}] \simeq 1.0$ ,  $[\text{Fe}/\text{H}] \simeq 0.5$ ), found by us in HD 188101 (see Section 5) on the determination of  $T_{\text{eff}}$  and  $\theta$ . The fluxes  $F_\lambda$  were calculated in the model with a modified chemical composition, which led to a change in  $T_{\text{eff}}$  by +40 K and  $\theta$  by  $-0.7 \mu\text{as}$  ( $\sigma_{abun}$  in Table 6). The final values of  $T_{\text{eff}}$  and the angular diameter corresponding to  $E(\text{B-V}) = 0.05$ , and the errors in the stellar parameters are given in Table 6. In Fig. 6 the theoretical fluxes for the ultimately adopted model are compared with the observations. Note that with the derived color excess and  $T_{\text{eff}}$  the deviation  $\sigma^m = 0.18$  does not differ greatly from the minimum  $\sigma^m = 0.17$ .

Table 6: The errors in  $T_{\text{eff}}$ , the angular diameter, and  $\log g$  for HD188101 and the final values of the stellar parameters

	$T_{\text{eff}}$ (K)	$\theta$ ( $\mu\text{as}$ )		$\log g$
	14200	67.5		3.70
$\sigma_E$	800	1.7	$\sigma_o$	0.05
$\sigma_g$	250	1.0	$\sigma_T$	0.15
$\sigma_O$	520	0.5	$\sigma_{\text{LTE}}$	-0.10
$\sigma_{abun}$	+40	-0.7	$\sigma_{abun}$	+0.02
$\sigma_{atm}$	990	2.0	$\sigma_{atm}$	0.16

Let us now determine  $\log g$  from the H I lines whose wings are sensitive to  $\log g$  at  $T_{\text{eff}} > 10000$  K. We computed a grid of model atmospheres using the LLmodels code and He I line profiles using the SynthVb code for a set of  $T_{\text{eff}}$  and  $\log g$ . The  $\text{H}_\alpha$ ,  $\text{H}_\beta$ ,  $\text{H}_\gamma$  line profiles are in best agreement with the observations at  $\log g = 3.70$  (Fig. 7).

The uncertainties in the derived  $\log g$  are attributable to the errors in the observations  $\sigma_o$  and the effective temperature  $\sigma_T$  (Table 6). We also estimated the systematic error in  $\log g$  due to the neglect of the departures from LTE,  $\sigma_{\text{LTE}}$ . For this purpose, we compared the  $\text{H}_\beta$  profiles computed when abandoning the assumption of LTE using the TLUSTY code (T. Lanz and I. Hubeny, 2007) with  $T_{\text{eff}} = 15000$  K and  $\log g = 4.0$  with our LTE calculations for the same atmospheric parameters. Compared to non-LTE, the LTE profile is stronger in the wings and, therefore, the same observed profile is reproduced in our LTE calculations at a lower value of  $\log g$ , by 0.1 dex. In addition, using the LLmodels models with abundances typical for HD 188101 ( $[\text{Si}/\text{H}] \simeq 1.0$ ,  $[\text{Ti}/\text{H}] \simeq 1.0$ ,  $[\text{Fe}/\text{H}] \simeq 0.5$ ) leads to a slight increase in  $\log g$  by 0.02 dex ( $\sigma_{abun}$  in Table 6).

We also determined  $\log g$  for HD 188101 using MESA (Modules for Experiments in Stellar Astrophysics) evolutionary tracks (Modules for Experiments in Stellar Astrophysics, A. Dotter, 2016; J. Choi et al., 2016). Assuming the initial chemical composition to be solar, neglecting the rotation and the magnetic field, and using our estimates of the luminosity  $L/L_\odot = 360_{-200}^{+640}$  and  $T_{\text{eff}}$ , we estimated  $\log g = 4.03_{-0.35}^{+0.31}$  and the mass  $M/M_\odot = 4.13 \pm 0.77$ . The errors were found by the Monte Carlo method with specified normal  $\lg L/L_\odot$ ,  $T_{\text{eff}}$  distributions. Both methods lead to consistent values of  $\log g$ , within the error limits.

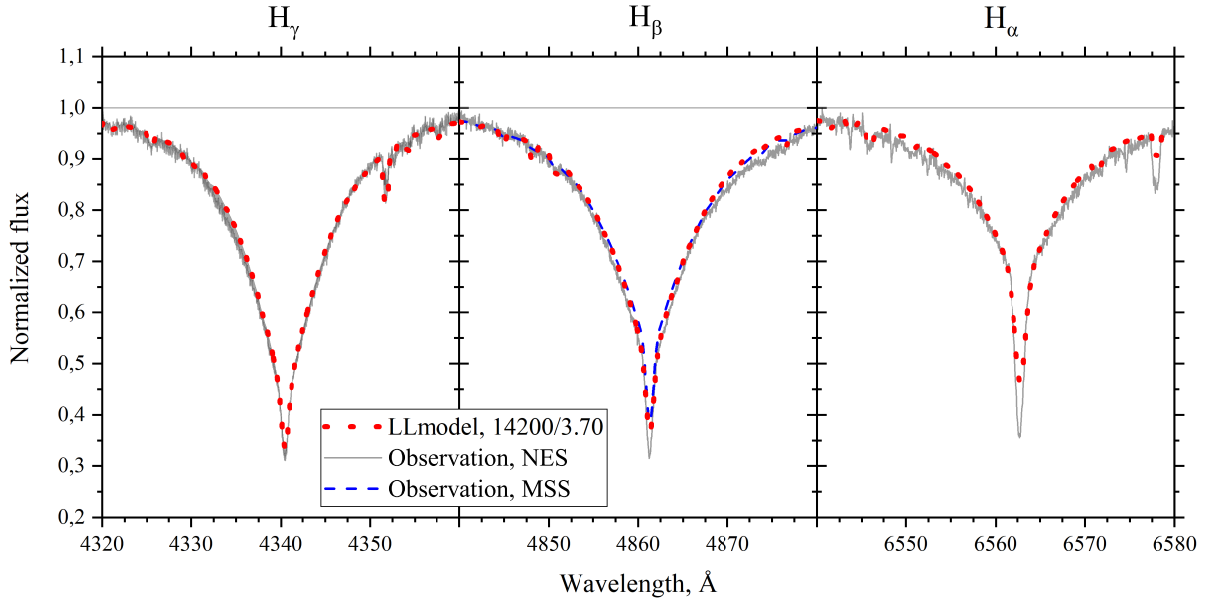


Figure 7: The theoretical hydrogen line profiles for the model with  $T_{\text{eff}} = 14200$  K and  $\log g = 3.70$  in comparison with the observed NES (solid curve) and MSS (dashed curve) spectra for HD 188101.

We did not find a sufficient number of weak and strong lines in the observed spectrum to determine the microturbulent velocity  $v_{\text{mic}}$  and took a value typical for CP stars,  $v_{\text{mic}} = 2.0 \text{ km s}^{-1}$ .

The parameters of HD 188101 derived in this paper and  $V \sin i$  and  $P$  taken from I. Yakunin et al. (2023) are presented in Table 7. The inclination of the rotation axis to the line of sight was calculated using  $V \sin i$ ,  $P$  and the radius.

## 5. CHEMICAL COMPOSITION

We determined the abundances from individual lines based on the MSS spectra and the NES spectrum for the lines uncovered by the MSS spectra. For the He I, Mg II, Si II, Si III and Ti II lines we made the determinations for two rotation phases, 0.4 and 0.9, based on the average spectra. In the first iteration we used the 14200/3.70 with  $v_{\text{mic}} = 2 \text{ km s}^{-1}$  and the solar chemical composition (K. Lodders, 2021), but it was subsequently recalculated using the abundances of individual elements (the Si, Ti, and Fe overabundances) derived in the first iteration. Our results are presented in Table 8. Figure 8 shows the mean LTE and non-LTE abundances  $[N_{\text{el}}/N_{\text{tot}}]$  for phases 0.4 and 0.9 (if the data are available). The He I 4471 Å line was not used in calculating the mean. To calculate  $[N_{\text{el}}/N_{\text{tot}}]$ , we used the protosolar abundances of elements from K. Lodders (2021).

Table 7: Parameters of the star HD 188101.

$T_{\text{eff}}(\text{K})$	$14200 \pm 990$
$\theta$ ( $\mu\text{as}$ )	$67.5 \pm 2.9$
$R/R_{\odot}$	$3.1^{+2.1}_{-0.9}$
$\log g$ (CGS)	$3.70 \pm 0.16$
$M/M_{\odot}$	$4.13 \pm 0.77$
$v_{\text{mic}}$ ( $\text{km s}^{-1}$ )	2.0
E(B-V)	$0.052 \pm 0.30$
r (pc)	$430^{+280}_{-120}$
$B_p$ (kG)	$<3.0$
$V\sin i$ ( $\text{km s}^{-1}$ )	33
$i$ ( $^{\circ}$ )	$42^{+19}_{-15}$
$P$ (days)	3.98726

Table 8: LTE (L) and non-LTE (N) abundances  $\lg(N_{\text{el}}/N_{\text{tot}})$  from individual lines in HD 188101 (14200/3.70 model) at two phases (0.4, 0.9) from the MSS spectra.  $E_{\text{exc}}$  is the lower-level excitation energy

Line	$E_{\text{exc}}$ , eV	lg gf	Phase 0.4			Phase 0.9		
			L	N	$[N_{\text{el}}/N_{\text{tot}}]$	L	N	$[N_{\text{el}}/N_{\text{tot}}]$
He I 4437	21.21	-2.03	-1.07	-1.09	-0.04			
He I 4713	20.96	-1.03	-1.20	-1.27	-0.22	-1.30	-1.36	-0.31
He I 5015 <sup>1</sup>	20.62	-0.82	-1.51	-1.61	-0.56			
C II 4267*	18.05	0.96	-3.10	-3.13	0.35			
N II 4607	18.46	-0.52	-3.27		0.83			
N II 4613	18.47	-0.69	-3.32		0.78			
N II 4630	18.48	0.08	-3.38		0.72			
N II 4643	18.48	-0.37	-3.17		0.93			
Mean			-3.29(09)		0.81			
O I 5329*	10.74	-1.24	-3.32	-3.43	-0.21			
O I 6155*	10.74	-0.66	-3.67	-3.84	-0.62			
O I 6158*	10.74	-0.30	-3.65	-3.83	-0.61			
Mean			-3.55(20)	-3.70(23)	-0.48			
Mg II 4427	10.00	-1.21	-4.37	-4.34	0.09			
Mg II 4433	10.00	-0.91	-4.39	-4.35	0.08			
Mean			-4.38(01)	-4.35(01)	0.08			
Mg II 4481	8.86	0.99	-4.97	-5.09	-0.66	-5.48	-5.50	-1.07
Al II 4663	10.60	-0.28	j-6.59		j-1.02			
Al II 6231*	13.07	0.52	j-6.59		j-1.02			
Al II 6243*	13.08	0.74	j-6.59		j-1.02			
Al III 4512	17.81	0.41	-5.60		-0.03			

Si II 4673	12.84	-0.34	-4.36	-4.10	0.34	-3.94	-3.64	0.80
Si II 5041*	10.07	0.15	-4.78	-3.87	0.57			
Si II 5055*	10.07	0.53	-5.06	-4.21	0.23			
Mean			-4.73(29)	-4.06(14)	0.38			
Si III 4552	19.02	0.18	-3.44	-3.64	0.80	-2.97	-3.25	1.19
Si III 4567	19.02	-0.04	-3.56	-3.71	0.73	-3.05	-3.28	1.16
Si III 4574	19.02	-0.51	-3.44	-3.54	0.90	-2.87	-3.04	1.40
Mean			-3.48(07)	-3.63(09)	0.81	-2.96(09)	-3.19(13)	1.25
P II 4499	13.38	0.61	-6.43		0.09			
Ti II 4443	1.08	-0.71	-6.18	-5.98	1.07			
Ti II 4501	1.12	-0.77	-6.05	-5.86	1.19			
Ti II 4563	1.22	-0.69	-6.27	-6.05	1.00	-6.11	-5.89	1.16
Ti II 4571	1.57	-0.31	-6.17	-6.00	1.05	-6.05	-5.89	1.16
Mean			-6.17(08)	-5.97(07)	1.08			
Cr II 4558	4.07	-0.37	-6.34		-0.02			
Cr II 4588	4.07	-0.65	-6.44		-0.12			
Cr II 4634	4.07	-1.05	-6.29		0.03			
Cr II 4824	3.87	-0.92	-6.17		0.15			
Mean			-6.31(11)		0.01			
Fe II 4508	2.85	-2.09	-4.89		-0.39			
Fe II 4522	2.84	-2.03	-4.94		-0.44			
Fe II 4555	2.83	-2.16	-4.84		-0.34			
Fe II 4583	2.81	-1.86	-4.72		-0.22			
Mean			-4.83(11)		-0.33			
Fe III 4431	8.25	-2.57	-3.83		0.67			
Fe III 5127*	8.66	-2.03	-3.66		0.84			
Fe III 5156*	8.64	-1.99	-4.11		0.39			
Mean			-3.87(23)		0.63			
Ni II 5050*	12.46	0.24	-4.34		1.41			
Sr II 4077*	0.00	0.14	-7.43	-7.34	1.73			
Sr II 4215*	0.00	-0.17	-6.98	-6.89	2.18			
Mean			-7.21(32)	-7.12(32)	1.95			

In parenthesis  $100 \cdot \sigma$ (dex).

<sup>1</sup> From the MSS spectra at phases 0.1-0.3.

\*From the NES spectrum.

In addition to the random errors  $\sigma$  due to the scatter in the abundances from different lines given in Table 8, we estimated the changes in the mean abundance due to the error in  $T_{\text{eff}}$ . Our LTE (or non- LTE, if the model atom is available) calculations were carried out for the model with  $T_{\text{eff}} = 15200$  K without any change in other atmospheric parameters. An increase in  $T_{\text{eff}}$  by 1000 K led to a change in the abundance by  $-0.20$ ,  $-0.26$ , and  $-0.27$  dex for He I 4437 Å, 4713 Å and 5015 Å,  $-0.33$  dex for N II, by  $+0.12$  dex for Mg II 4427 and 4433 Å, by  $+0.16$  dex for Mg II 4481 Å, by  $+0.26$  dex for Si II, by  $-0.34$  dex for Si III, by  $+0.32$  dex for Fe II, and by  $-0.09$  dex for Fe III.

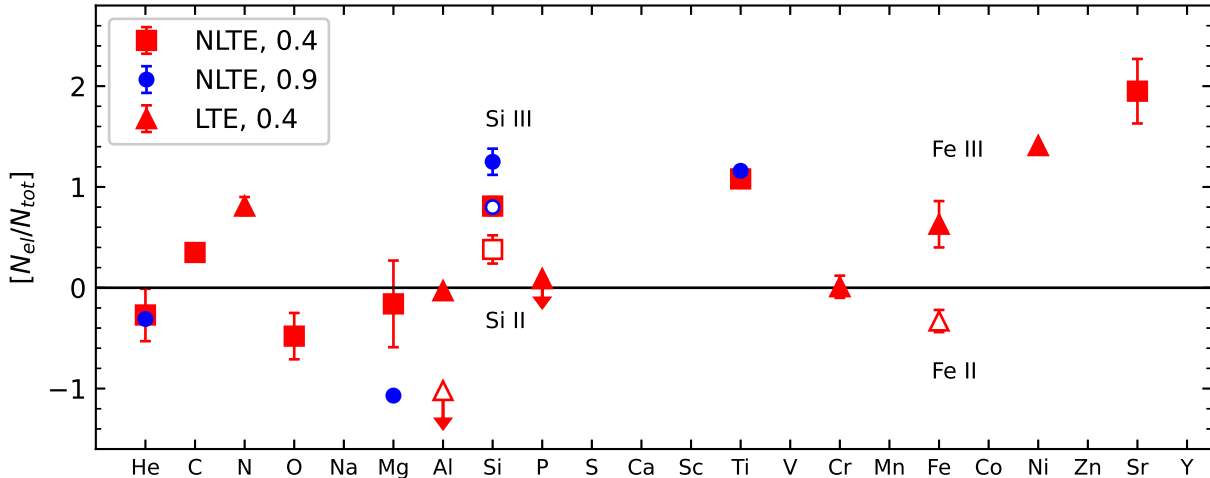


Figure 8: The chemical composition of HD 188101. The Al, Si, and Fe abundances from the lines of the II (unfilled symbols) and III (filled symbols) ionization stages are given. The arrows indicate the upper limits. The error bar indicates the dispersion of the abundance when averaged over all lines of the element.

It turned out to be impossible to reproduce the He I 4471 Å and 4921 Å line profiles neither under the assumption of LTE nor when abandoning it. Figure 9 shows the theoretical profiles that agree best with the observations in the line wings and core for He I 4471 Å. The He abundance difference between these two cases is 0.6 dex. The profile computed with the solar abundance is shown for comparison. We derived the solar abundance from the weak Mg II 4427 and 4433 Å lines and an underabundance of  $-0.74$  dex from the strong Mg II 4481 Å line. For Si, Fe, and Al in the LTE approximation the abundances from the lines of the II and III ionization stages differ by  $\simeq 1$  dex. The Si II and Si III lines have non-LTE corrections of opposite signs and, therefore, the abundance difference between Si II and Si III decreases in our non-LTE calculations. It is completely removed by raising  $T_{\text{eff}}$  by  $\simeq 700$  K, which is within the temperature error limits. We suggest that a non-LTE analysis is needed to reconcile the abundances from the Al II and Al III lines and from the Fe II and Fe III lines.

Large Si, Ti, and Sr overabundances are observed in HD 188101, and there is a hint at a He underabundance. Note that no criterion has been established in the literature for the He underabundance in He-weak stars. Based on such observational manifestations typical for He-weak stars as Si, Ti, and Sr overabundances, a possible slight He underabundance, and a weak magnetic field, we classify HD 188101 as a He-weak SiTiSr star.

## 6. DISCUSSION

The change in line absorption with rotation phase, the different abundances from different lines of the same species for the same phase, and the impossibility of reproducing the He I 4471 and 4921 Å line profiles within the classical model atmosphere suggest that

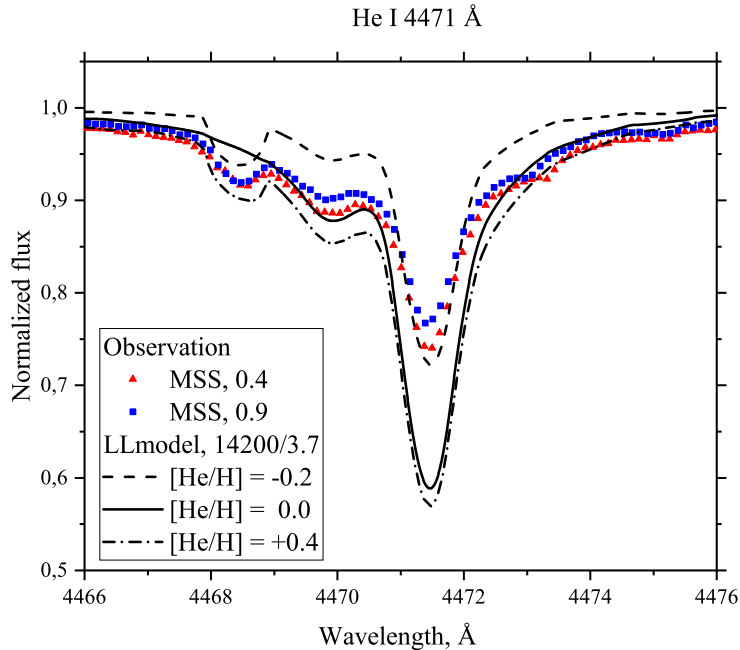


Figure 9: Demonstration of the impossibility of describing the He I 4471 Å profile (the triangles and squares represent the MSS spectra at phases 0.4 and 0.9, respectively) within the framework of a homogeneous model, without taking into account the stratification and spots. The synthetic spectra were constructed in non-LTE with various  $[\text{He}/\text{H}]$  abundances.

the surface layers are inhomogeneous in chemical composition. We assumed the presence of spots on the surface that create the observed features due to the stellar rotation. Based on the light curve (Fig. 10, the upper panel), we found the distribution of the intensity emerging along the normal over the stellar surface by the Tikhonov regularization method (Fig. 10, the lower panel). The dashed line marks the boundary below which the stellar surface is not observed. For details, see, e.g., A. Kolbin et al. (2013). Spots with different intensities  $\simeq 60^\circ$  in size typical for CP stars can be seen.

With the help of the LLmodels code and the convolution with the Kepler transmission curve, we computed the corresponding fluxes for phases 0.4 and 0.9 using the previously derived elemental abundances for them. The right arrow on the upper panel of Fig. 10 indicates the difference of these fluxes. It can be seen that the scales of the brightness variations correspond to the flux variations due to the abundance variations. Note that the change in absorption beyond the ionization threshold of the ground Si I level ( $\lambda = 1528 \text{ \AA}$ ) plays the main role in the flux variations. The flux in the far ultraviolet decreases with increasing Si abundance and increases in a longer-wavelength range.

Consider the variability of the He I 4713 Å line equivalent width within the simplest model. Assuming the spot to be an equatorial spherical circle and the fluxes in the continuum of the spot and outside it to be identical, we estimated the spot sizes and position on the surface (the solid curve in Fig. 11) and the  $[\text{He}/\text{H}]$  abundance in (from

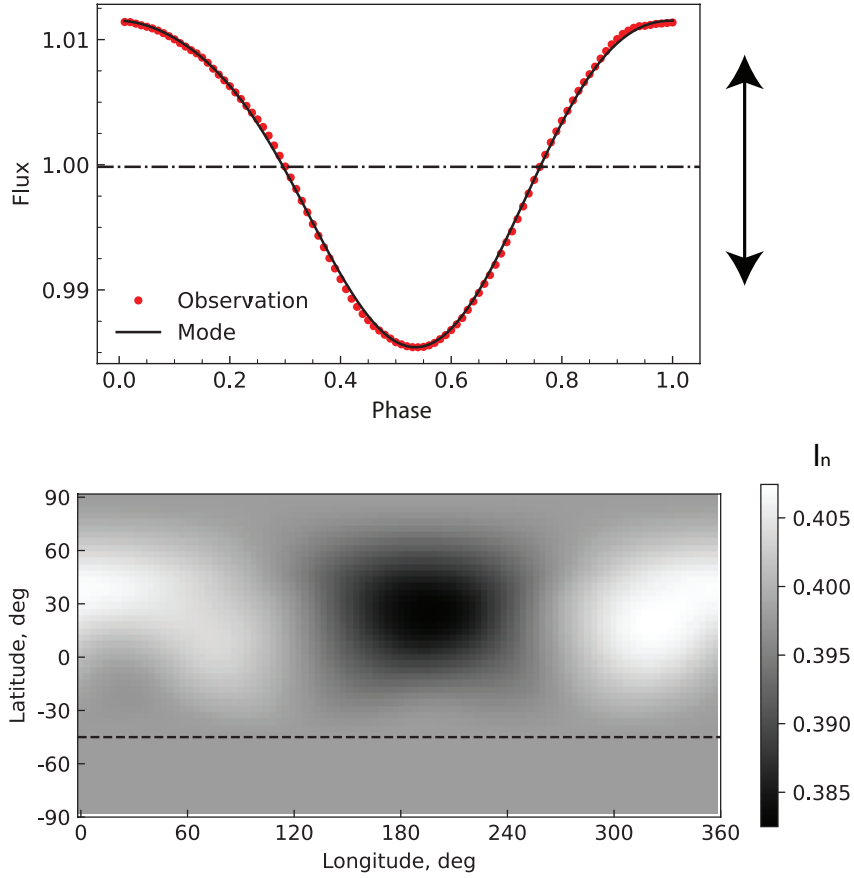


Figure 10: Upper panel: the light curve of HD 188101 in the Kepler filter (dots) in comparison with the model light curve (solid line). Lower panel: the derived intensity distribution.

0.0 to +0.1) and outside (from  $-0.2$  to  $-0.4$ ) the spot. Just as from the light curve, we obtained a spot size typical for peculiar stars,  $\simeq 60^\circ$ . This analysis points to the need for applying more complex models, such as those in Y. Pakhomov et al. (2024); I. Potravnov et al. (2024). The element on the stellar surface being resolved by MSS has an extent in longitude  $\Delta l^\circ = 90^\circ \times c/R/V \sin i \simeq 60^\circ$ . Therefore, observations using an instrument with a resolution  $R > 60\,000$  is required for Doppler mapping.

Thus, a nonuniform distribution of chemical elements over the surface, typical for peculiar stars, is most likely responsible for the variability of the brightness and absorption in spectral lines. Within a simple model we obtained the He abundance spot and the intensity at phase 0.4. Our abundance analysis at this phase led to an elemental abundance closer to the solar one compared to that at phase 0.9, where the Si spot is located.

The He I 4471 and 4921 Å line profiles are not reproduced irrespective of the phase. The non-LTE effects cannot be responsible for the strong wings and the weak core of the observed profile relative to the theoretical one. This may argue for vertical He stratification

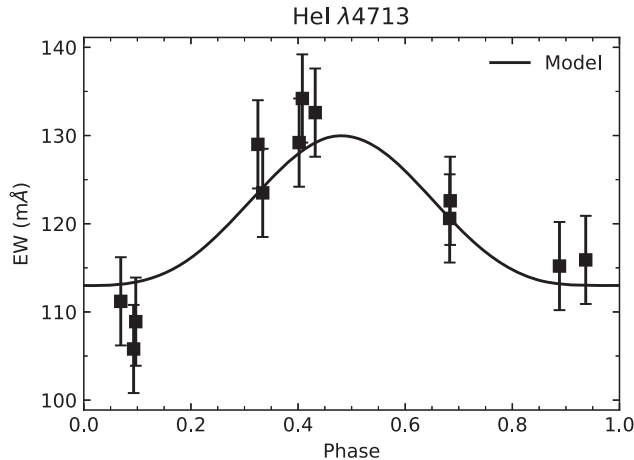


Figure 11: Change in the He I 4713 Å equivalent widths with rotation phase (squares). The curve corresponds to the model with a circular equatorial spot.

or a more complex spot structure.

## 7. CONCLUSIONS

Based on our analysis of the spectroscopic time series and photometric data, we determined the atmospheric parameters of the star HD 188101 with a weak magnetic field ( $|B_z| < 1$  kG, I. Yakunin et al., 2023):  $T_{\text{eff}} = 14200 \pm 990$  K and  $\log g = 3.70 \pm 0.16$ . The surface gravity derived from the profiles of Balmer H I lines agrees, within the error limits, with  $\log g$  derived from evolutionary tracks. The profiles are well described at  $T_{\text{eff}}$  determined from photometric observations, suggesting that  $E(B-V)$  obtained from interstellar extinction maps is correct. The parameters derived by us are consistent with the results of I. Yakunin et al. (2023), 14700/3.8.

We constructed a model He I atom. Even our non-LTE calculations do not allow the He I 4471 and 4921 Å line profiles to be reproduced within the framework of a classical, homogeneous model atmosphere, while the He I 4437, 4713, and 5015 Å lines give different abundances for the same rotation phase, but in all of the cases there is an underabundance of He relative to its solar abundance, from  $-0.04$  to  $-0.56$  dex.

We carried out non-LTE calculations for C II, O I, Mg II, Si II/Si III, Ti II, and Sr II. The Mg II 4427 and 4433 Å lines give a nearly solar abundance, while Mg II 4481 Å gives a value lower by 0.74 dex. The non-LTE abundances from the Si II and Si III lines can be reconciled if we raise  $T_{\text{eff}}$  by  $\simeq 700$  K, which is within the temperature error limits. Overabundances of Si, Ti, and Sr with  $[\text{Si}/\text{H}] \simeq 1.0$ ,  $[\text{Ti}/\text{H}] = 1.12$  and  $[\text{Sr}/\text{H}] = 1.95$  were revealed in the star.

Thus, judging by its chemical composition, HD 188101 belongs to the Bp class, the group of He-weak SiTiSr stars, and shows photometric variability and absorption in the He I, Mg II, Si II, Si III, Ti II, and Fe II lines typical for peculiar stars. The changes of

the absorption in the He I and Mg II 4481 Å lines anticorrelate with the absorption in the Si II, Si III, Ti II, and Fe II lines.

To understand the causes of the photometric and spectroscopic variability of HD 188101, to reproduce the profiles of strong He I lines, and to remove the discrepancies in the abundances from different lines of the same element, it is necessary to model the surface layers and radiative transfer by taking into account the chemical inhomogeneity and to obtain a series of high-resolution spectroscopic observations uniformly distributed in rotation phases.

**Acknowledgments.** The work presented in Subsections 3.2 and 3.3 was performed within RSF project no. 23-12-00134. The work performed in Section 2 was supported by RSF grant no. 25-12-00003. We used the NIST, NORAD, Simbad, TOPbase, VALD, and ADS<sup>14</sup> databases. We are grateful to I. S. Potravnov for the consultations in working with the spectroscopic time series.

## References

- S. Alexeeva et al., *Mon. Not. Roy. Astron. Soc.* **462** (1), 1123 (2016).
- S. Alexeeva et al., *Astrophys. J.* **866** (2), 153 (2018).
- F. Arenou et al., *Astron. Astrophys.* **258**, 104 (1992).
- L. Auer and D. Mihalas, *Astrophys. J. Suppl. Ser.* **25**, 433 (1973).
- A. J. Barnard, J. Cooper, E. W. Smith, *JQSRT* **14**, 1025 (1974).
- K. Butler, Ph.D. Thesis, University of London (1984).
- E. Borra et al., *Astrophys. J. Suppl. Ser.* **53**, 151 (1983).
- I. Bray et al., *Astron. Astrophys. Suppl. Ser.* **146**, 481 (2000).
- H. van Regemorter, *Astrophys. J.*, **136**, 906 (1962).
- S. Ghazaryan et al., *Mon. Not. Roy. Astron. Soc.* **487** (4), 5922 (2019).
- Gaia Collab., *Astron. Astrophys.* **649**, A1 (2021).
- Gaia Collab., *VizieR Online Data Catalog I/355* (2022).
- J. Giddings, Ph.D. Thesis, University of London (1981).
- The HIPPARCOS and TYCHO catalogues, *ESA Special Publication*, vol. 1200 (1997).
- G. Gontcharov, *Astronomy Letters* **43** (7), 472 (2017).

---

<sup>14</sup>[http://adsabs.harvard.edu/abstract\\_service.html](http://adsabs.harvard.edu/abstract_service.html)

- H. R. Griem, Spectral line broadening by plasmas, Academic Press New York and London (1974).
- G. Green et al., *Astrophys. J.***887** (1), 93 (2019).
- A. Dotter, *Astrophys. J. Suppl. Ser.***222** (1), 8 (2016).
- A. Deutsch, *Astrophys. J.***116**, 536 (1952).
- P. Dufton, C. McKeith, *Astron. Astrophys.***81**, 8 (1980).
- A. Kolbin et al., *Astronomy Reports* **57** (7), 548 (2013).
- S. Korotin and T. Ryabchikova, *Astronomy Letters* **44** (10), 621 (2018).
- O. Kochukhov et al., *Astron. Astrophys.* **433** (2), 671 (2005).
- O. Kochukhov, *Astrophysics Source Code Library*, record ascl:1805.015 (2018)
- A. Kramida et al., NIST ASD Team, NIST Atomic Spectra Database (version 5.10). Gaithersburg MD, USA (2022).
- W. Cunto et al., *Astron. Astrophys.* **275**, L5 (1993).
- R. Cutri et al., *VizieR Online Data Catalog: 2MASS All-Sky Catalog of Point Sources (Cutri+ 2003)*, *VizieR On-line Data Catalog: II/246*. Originally published in: 2003yCat.2246....0C (2003).
- R. Cutri et al., *Explanatory Supplement to the WISE All-Sky Data Release Products*, *Explanatory Supplement to the WISE All-Sky Data Release Products* (2012).
- R. Lallement et al., *Astron. Astrophys.***661**, A147 (2022).
- T. Lanz and I. Hubeny, *Astrophys. J. Suppl. Ser.***169** (1), 83 (2007).
- F. Leone et al., *Astron. Astrophys.***293**, 457 (1995).
- K. Lodders, *Space Sci. Rev.* **217**, id.44 (2021).
- L. Mashonkina et al., *Mon. Not. Roy. Astron. Soc.* **499**, 3706 (2020).
- L. Mashonkina, *Mon. Not. Roy. Astron. Soc.* **493** (4), 6095 (2020).
- J. Mathis, *Ann. Rev. Astron. Astrophys.***28**, 37 (1990).
- G. Michaud, 1970, *Astrophys. J.* **160**, 641 (1970)
- G. Michaud et al., *Atomic Diffusion in Stars* (2015).
- S. N. Nahar, *New Astronomy* **15**, 417 (2010).
- M.-F. Nieva, N. Przybilla, *Astron. Astrophys.* **539**, A143 (2012).

- J. Norris, *Astrophys. J. Suppl. Ser.* **23**, 213 (1971).
- Y. Pakhomov et al., *Universe* **10** (9), 341 (2024).  
Y. Pakhomov, *Astronomy Letters* **50** (1), 34 (2024).
- I. Potravnov et al., *Mon. Not. Roy. Astron. Soc.* **527** (4), 10376 (2024).  
G. W. Preston, *mn. Rev. Astron. Astrophys.* **12**, 257
- N. Przybilla, *Astron. Astrophys.* **443** (1), 293 (2005).
- N. Przybilla, M.-F. Nieva, K. Butler, *Journal of Physics Conference Series*, **328**, 012015 (2011).
- I. Romanyuk, *Astrophysical Bulletin* **62** (1), 62 (2007).
- T. Ryabchikova et al., *Phys. Scr.* **90**, 054005 (2015).  
T. Ryabchikova et al., *Mon. Not. Roy. Astron. Soc.* **456**, 1221 (2016).
- N. Sakhbullin and W. Schabert, *Soviet Astronomy Letters* **16**, 231 (1990).  
J. Sikora et al., *Mon. Not. Roy. Astron. Soc.* **498** (2), 2456 (2020).
- T. Sitnova et al., *Astronomy Letters* **39** (2), 126 (2013).
- T. Sitnova et al., *Astronomy Letters* **46** (2), 120 (2020).
- M. J. Seaton, in *Atomic and Molecular Processes* (New York: Academic Press) (1962).
- P. Sawey, K. Berrington, *Atomic Data and Nuclear Data Tables* **55**, 81 (1993).
- Y. Takeda, *Publ. Astron. Soc. Japan* **46**, 181 (1994).
- G. Thompson et al., *Catalogue of stellar ultraviolet fluxes : a compilation of absolute stellar fluxes measured by the Sky Survey Telescope (S2/68) aboard the ESRO satellite TD-1 /* (1978).
- G. Topil'skaya, *Bulletin of the Special Astrophysics Observatory* **36**, 52 (1993)
- S. Hümmerich et al., *Astron. Astrophys.* **619**, A98 (2018).
- D. Husfeld et al., *Astron. Astrophys.* **222**, 150 (1989).
- V. Tsymbal, T. Ryabchikova, T. Sitnova, in Kudryavtsev D.O., Romanyuk I.I., Yakunin I.A., eds, *Astron. Soc. Pacific Conf. Ser.* **518**. *Physics of Magnetic stars*, San Francisco: Astronomical Society of the Pacific, 247 (2019)
- M. Fukugita et al., *Astron. J.* **111**, 1748 (1996).
- K. Chambers et al., arXiv e-prints arXiv:1612.05560 (2016).
- J. Choi et al., *Astrophys. J.* **823** (2), 102 (2016).
- D. Shulyak et al., *Astron. Astrophys.* **428**, 993 (2004).
- I. Yakunin et al., *Astrophysical Bulletin* **78**, 141 (2023).